The structure of a magnetic-field front propagating non-diffusively in low-resistivity multi-species plasma

B. Rubinstein, R. Doron, Y. Maron, A. Fruchtman, and T. A. Mehlhorn

---

Articles you may be interested in

Some aspects of the double layer structure in magnetized electronegative plasmas with q-nonextensive electrons
Phys. Plasmas **22**, 112110 (2015); 10.1063/1.4935698

Measurements and modeling of the impact of weak magnetic fields on the plasma properties of a planar slot antenna driven plasma source
J. Vac. Sci. Technol. A **33**, 031303 (2015); 10.1116/1.4916018

Solitary structures in a spatially nonuniform degenerate plasma in the presence of quantizing magnetic field
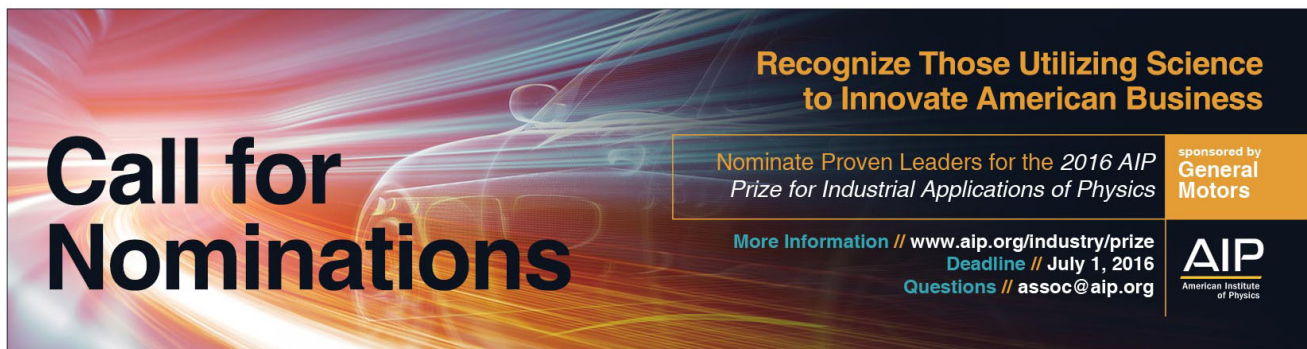Phys. Plasmas **22**, 032305 (2015); 10.1063/1.4914859

Measuring the magnetic field of a magnetized plasma using Raman scattering
Appl. Phys. Lett. **104**, 141107 (2014); 10.1063/1.4868870

Observation of faster-than-diffusion magnetic field penetration into a plasma
Phys. Plasmas **10**, 112 (2003); 10.1063/1.1527630

The structure of a magnetic-field front propagating non-diffusively in low-resistivity multi-species plasma

B. Rubinstein,[1] R. Doron,[1,a)] Y. Maron,[1] A. Fruchtman,[2] and T. A. Mehlhorn[3]
[1]*Weizmann Institute of Science, Rehovot 76100, Israel*
[2]*H.I.T.-Holon Institute of Technology, Holon 58102, Israel*
[3]*Plasma Physics Division, Naval Research Laboratory, Washington, DC 20375, USA*

We report on the first experimental verification of the traveling-wave-like picture of a magnetic-field and an associated electric potential hill propagating non-diffusively in low resistivity plasma. High spatial resolution spectroscopic method, developed here, allowed for obtaining the detailed shape of the propagating magnetic-field front. The measurements demonstrated that the ion separation, previously claimed, results from the reflection of the higher charge-to-mass ratio ions from the propagating potential hill and from climbing the hill by the lower charge-to-mass ratio ions. This ion dynamics is found to be consistent with the observed electron density evolution. *Published by AIP Publishing.* [http://dx.doi.org/10.1063/1.4947220]

Magnetic field propagation in low-resistivity plasmas and anomalous plasma transport across magnetic fields are key issues in plasma physics and astrophysics. In laboratory plasmas, these are dominant processes in magnetic fusion devices,[1] theta pinches,[2,3] ion diodes,[4] plasma switches,[5] and in plasma-beam transport across magnetic fields.[6] In space and astrophysics, plasma transport across magnetic fields greatly affects the interaction of the solar wind with the earth's magnetic field,[7] the evolution of solar flares,[8] the coronal heating,[9] and the evolution of accretion discs.[10]

Understanding the magnetic-field penetration into the plasmas on time-scales much shorter than expected from a classical diffusion is a long-standing problem. Early experimental evidence of such unexpectedly fast magnetic-field penetration into low-resistivity plasma (e.g., Refs. 11 and 12) was a subject of controversy. Later, experimental studies,[13–15] based on the spectroscopic measurements, have proved the fast field penetration. Spectroscopic measurements[16] indicated that fast magnetic field penetration was induced by the Hall electric field, as suggested by the theory based on electron-magneto-hydrodynamics[17–21] rather than by anomalous resistivity. Interferometric[22,23] and spectroscopic[15] measurements have also shown the propagation of an electron density rise followed by a significant drop. Additionally, early simulations[24–26] and models[27] pointed out to the possibility of a developing potential that could result in ion separation. Indeed, later experiments revealed complex ion dynamics.[28,29] In particular, ion separation was demonstrated in which light ions are specularly reflected by the magnetic field, while the heavy-ion plasma is penetrated.[28] A detailed picture of the evolution of the magnetic field is essential to determine the wave-like vs. diffusive characteristics of the magnetic field penetration. It is also critical for determining and understanding the width of the current layer and for a coherent description of the ion dynamics.

In previous studies,[14,15] the magnetic field was measured using Zeeman splitting, and the density and ion velocities using line emission intensities and Doppler shifts. Three major difficulties in those measurements prevented the progress. First, the low light-intensities emitted from the low density plasma prohibited a reliable analysis of Zeeman-dominated line-shape without compromising the spatial and temporal resolutions. Second, the large gradients in the plasma properties that develop along the field propagation direction interrupt the Doppler-shift measurements. Third, the irreproducibility that characterizes transient plasma systems requires simultaneous measurements of several parameters.

This letter presents a self-consistent experimental picture of the magnetic-field propagation through multi-ion, low-resistivity plasma, inferring the detailed shape of the magnetic-field-front penetrating the low charge-to-mass ratio plasma component, non-diffusively, in the form of a traveling wave. In particular, this is the first time that the existence of an electric-potential hill inside the plasma and its form are determined. The shape of the potential demonstrates that the previously discovered ion separation follows naturally and self-consistently the potential and magnetic-field evolution.

We developed a spectroscopic approach for inferring the magnetic field based on simultaneous measurements of the time evolution of the ion-velocity and electron density across the field front. Information on the ion dynamics and propagating magnetic field was obtained with high sensitivity and with sub-mm spatial resolution, which approaches the plasma electron skin-depth ($350\,\mu$m), the lowest expected current-layer width.

In the configuration studied, schematically described in Fig. 1, a pulsed current that rises to 130 kA in $\sim$350 ns and generates the magnetic field is driven through a multi-ion species plasma (mainly protons and carbon ions) that prefills the volume between two planar, 14-cm wide, electrodes. The

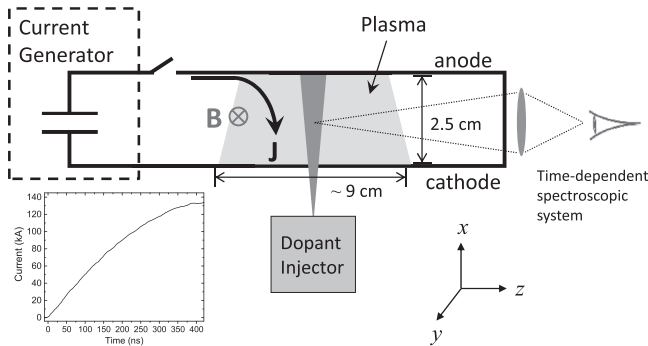a)Author to whom correspondence should be addressed. Electronic mail: ramy.doron@weizmann.ac.il

FIG. 1. Schematics of the experimental setup. J denotes the current. The magnetic field (B) propagates from the current-generator side edge of the plasma along z. A trace of the upstream current is shown on the lower left side of the figure.

plasma source, located above the anode, generates a density gradient across the anode-cathode (A-K) gap that supports Hall-field induced penetration. The initial electron density and temperature, prior to the current application are, respectively, $n_e = 2 \times 10^{14}\,\mathrm{cm}^{-3}$ and $T_e = 6.5\,\mathrm{eV}$. Radiation emitted from the plasma is imaged on a 1-m spectrometer input slit. The spectrometer output is conveyed to an array of fast (rise-time 3 ns and exponential fall-time of 6 ns) photo-multipliers (PMTs). A detailed description of the experimental set-up and the current pulse can be found in Refs. 15 and 30. A laser blow-off technique[31] was employed for controlled dopant injection (along x) into the y-center of the A-K gap. We achieved nearly uniform, low-density (peak ion densities $< 1.5 \times 10^{13}\,\mathrm{cm}^{-3}$), non-perturbative dopant columns of widths between 2 and 5 mm (FWHM).

In our low-beta plasma, the electric force that accelerates the unmagnetized ions equals the magnetic force on the whole plasma, which is proportional to the magnetic field gradient. Thus, the ion velocity evolution can serve as a probe for the shape of the magnetic field. As described below, this approach also enables us to achieve spatial resolution that is better than the width of the dopant column. In the present experiment, boron is used as a dopant, mainly utilizing the B II $2s - 2p$ emission (3451 Å). Despite the small width of the dopant column, it was found to accommodate density and temperature gradients generated by the propagating magnetic-field, which caused complex spectral line-shapes, prohibiting a reliable measurement of the B II velocity via a naive attempt to determine the mean Doppler-shift. Instead, we tracked the intensity evolution of discrete components of the line shape; each component is Doppler-shifted corresponding to a different ion velocity. The intensity evolution of such four different monochromatic components of the time-dependent B II $2s - 2p$ line shape is presented in Fig. 2(a). Each of the Doppler-shifted intensity rises and then drops in time. The times of the beginning of the intensity rises are when the ions at the upstream side of the dopant column acquire their corresponding velocities. It will be shown that these times are the arrival times of corresponding magnetic-field magnitudes.

The time-dependent Doppler-shift intensities were normalized and time-shifted, so that their peaks coincide, as shown in Fig. 2(b). It is seen that all of the normalized
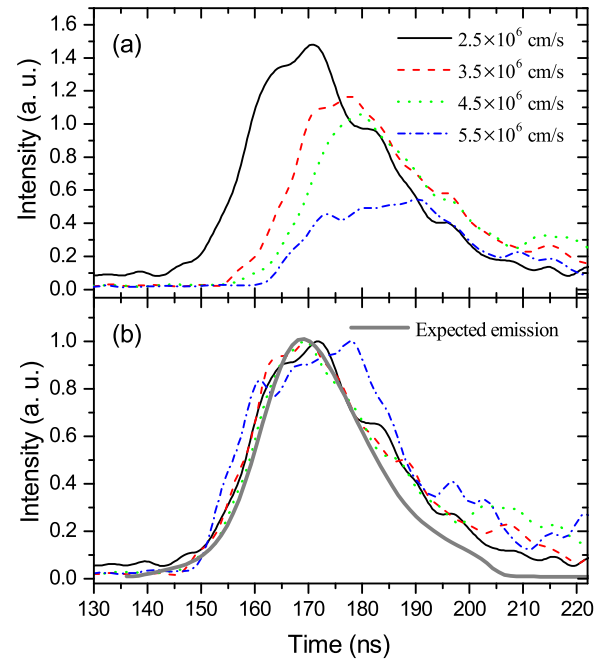

FIG. 2. (a) The intensity evolution of selected Doppler-shifted components of the B II $2s - 2p$ transition (3451 Å). The ion velocities corresponding to each of the curves are given in the legend. (b) The curves presented in (a), normalized and shifted to a common center, together with the normalized emission expected from a Doppler-shifted component propagating at a velocity of $3 \times 10^7\,\mathrm{cm/s}$ through the dopant column, convolved with the PMT temporal response. *Time* $= 0$ represents the beginning of the current pulse.

intensity evolutions nearly overlap. Therefore, we define a dopant ion-velocity field that can be described in terms of a traveling wave: $v_i(z, t) = v_i(z - v_b t)$, where v_i is the dopant ion velocity. The wave velocity v_b was determined using the dopant-ion density distribution, based on the images taken prior to the magnetic field application. Since the light intensity distribution in the image is proportional to the dopant-ion density, we can simulate the expected time-evolution of the Doppler-shifted emissions by dividing the density distribution spatial scale by the wave velocity and convolve the result with the PMT response function. In the measurement presented in Fig. 2, the dopant column FWHM was 4.3 mm, yielding $v_b = 3 \times 10^7\,\mathrm{cm/s}$, required to obtain the agreement between the normalized Doppler-shifted intensity evolutions and the expected emission evolution seen in 2(b). Deviations from the expected emission, mainly seen at late times and for the large Doppler shifts, are due to a lower signal-to-noise ratio and emission from impurities. The latter is verified in experiments performed with no doping. The measurement integration along the x direction was 250 μm. Measurements performed in different discharges yielded similar results to $\sim$15 %. Thus, in light of the irreproducible nature of such pulsed-power systems it is reasonable to assume that the velocity changes rather slowly around the point of observation.

The evolution of the dopant-ion velocities as a traveling wave implies that the accelerating force on the ions also evolves as a wave. The ions are unmagnetized and collisionless, and therefore, it is an electric field that propagates in the plasma as a traveling wave. In the wave reference-frame,

the dopant ions climb an electrostatic potential hill ϕ, and their total energy is conserved

$$\phi = \frac{m_i v_i^2}{2 Z_i e}\left(\frac{2 v_b}{v_i} - 1\right), \tag{1}$$

where m_i and Z_i denote the dopant ion mass and charge state, v_i is the dopant ion velocity in the laboratory frame, and e is the elementary charge. We note that the energy conservation assumption is justified since the transit time of the wave through the dopant is ~ 30 ns that is significantly shorter compared to the system evolution time of ~ 350 ns.

We now determine the B II velocity evolution $v_i(t)$ and use it to calculate the evolution of the electric potential. We define the point of observation to be the dopant-plume center. The time at which the B II at the plume center acquires a specific velocity is the time of the Doppler-shifted peak emission associated with this velocity. The peak times are determined by fitting each of the intensity evolutions by a Gaussian that was found to give an appropriate description of the phenomenon. Since these times are determined with an uncertainty $\lesssim 3$ ns (excluding the highest two velocities where the signal-to-noise ratios are higher), the corresponding spatial resolution, due to the wave velocity v_b, is less than 1 mm. Ten values of the potential at different times are calculated (Eq. (1)) for ten measured B II-velocities, from 0.5×10^6 to 9.5×10^6 cm/s, at the plume center. Figure 3 shows the evolution of the electric potential. Because of the traveling wave nature of the potential, its time evolution also represents its z-spatial profile. The non-monotonic feature seen in Fig. 3 (at ~ 185 ns) is discussed below.

Once the presence of a potential hill is established, the measured B II velocity can be used to calculate the dynamics of all other ion species. Furthermore, knowing the plasma composition, we can also derive the electron density evolution. In the wave reference frame, all plasma ions climb the potential hill. The jth ion-species velocity distribution function in the moving frame, prior to the arrival of the potential hill, is written as, $\tilde{f}_j(v_x, v_y, v_z) = g(v_x) h(v_y) f_j(v_z)$, where we

FIG. 3. The time evolution of the electric potential at the dopant-plume center, namely, at $x = 10$, $y = 0$, and $z = 35$ mm. The corresponding z-distribution (at $t = 160$ ns) is shown in the top horizontal axis.

choose g and h so that $\int_{-\infty}^{\infty} dv_x g(v_x) = \int_{-\infty}^{\infty} dv_y h(v_y) = 1$. Since the plasma ions are not magnetized and the electric field is assumed to be directed along the z axis, g and h do not vary along the ion trajectory and the density evolution of the ions follows the evolution of f_j. In the potential hill rest frame, all ions move towards it with an average velocity $-v_b$. We describe the initial ion z-velocity-distribution, due to the ion emission from the plasma source,[30] in the moving potential frame as

$$f_j(v_z) = (n_{j0}/2\Delta v_z)[H(v_z/v_b + 1 + \Delta v_z/v_b) \\ - H(v_z/v_b + 1 - \Delta v_z/v_b)], \tag{2}$$

where H is the Heaviside function. Here, n_{j0} is the density of the jth ion-species before the arrival of the potential hill. The spread of the prefilled plasma velocity in the z direction was measured to be $\Delta v_z \sim 10^6$ cm/s.[30] Including the initial ion velocities in the model contributes to the smearing out of the otherwise sharp density peaks at the points where ions are reflected off the propagating field front. While each ion species has somewhat different initial velocity distribution, these velocities are less than $0.1\times$ the magnetic-field propagation velocity. Therefore, considering a different velocity distribution for each species would have a negligible effect on the simulation results (which are further convolved with the detection system temporal response). The ion velocity distribution function is a function of the ion constants of motion and satisfies

$$f_j(v_z, \phi) = f_j\left(-\sqrt{v_z^2 + 2 Z_j e \phi / m_j}, \phi = 0\right). \tag{3}$$

Integrating the velocity distribution function, we obtain expressions for the jth ion density. In our experiment, each ion species experiences either full transmission or full reflection. The density distribution of the jth ion-species is then

$$n_j(\phi) = \frac{n_{j0} v_b}{(1+k)\Delta v_z}\left[\sqrt{\left(1 + \frac{\Delta v_z}{v_b}\right)^2 - \frac{2 Z_j e \phi}{m_j v_b^2}} \\ - l\sqrt{\left(1 - \frac{\Delta v_z}{v_b}\right)^2 - \frac{2 Z_j e \phi}{m_j v_b^2}}\right], \tag{4}$$

where for full transmission $k = l = 1$, while for full reflection $k = 0$ and $l = 1$. The details of the calculation are given elsewhere.[32] The ion densities (protons and C II-V) prior to the current pulse application are adopted from previous studies.[30]

Figure 4 shows the density profiles of the different species as a function of time. The peaks seen in the figure are the points of reflection of the various species. The protons are the first to be reflected. Then, C V and C IV are reflected, whereas C II and C III climb the entire potential. The predicted electron density is obtained by summing the calculated ion-species densities multiplied by their respective charge and convolved with the spectroscopic system response time. This simulated electron density is compared with an independent electron density measurement, based on
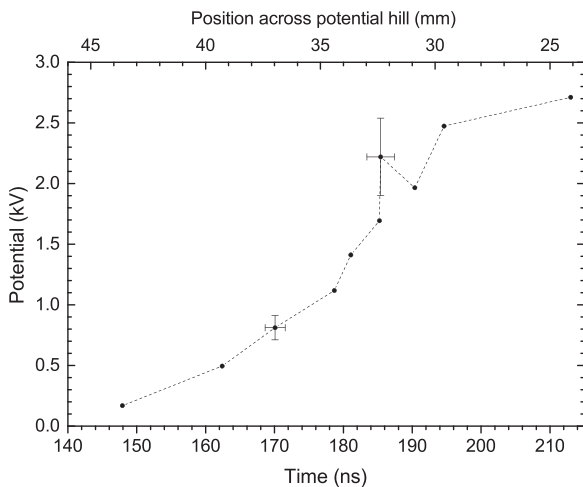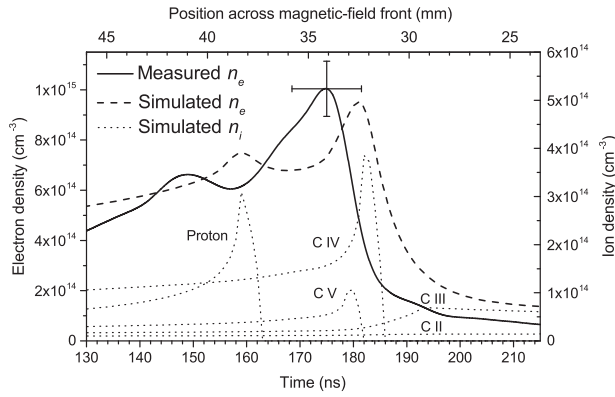
FIG. 4. The simulated density evolution of the various ion-species at the dopant-plume center and the resulting electron density evolution (convolved with the temporal response of the spectroscopic system), compared with an independent measurement of the electron density. The corresponding z-distribution ($t = 160$ ns) is shown in the top horizontal axis.

fitting the intensity evolutions of the $2s - 2p$ transitions in B II (3451 Å) and B III (2066 Å). A detailed description of the density measurement is given elsewhere.[32] The good agreement seen in the figure strongly supports the existence of an electric potential hill.

We now calculate the magnetic field profile. The plasma is highly conductive, so the accelerating electric field can be approximated as $E_z = -(B/e\mu_0 n_e)(\partial B/\partial z)$ (e.g., Ref. [19]), where μ_0 is the vacuum permeability. The magnetic field is then given by

$$B^2(\phi) = 2e\mu_0 \int_0^\phi n_e(\phi')d\phi', \qquad (5)$$

which can be expressed by quadratures, for the density written as a sum of terms of the form in Eq. (4). From Eq. (5), it follows that the transmission of ions across the potential hill is their penetration by the magnetic field, whereas the reflection from a certain potential height is a reflection from the corresponding magnetic-field amplitude. Figure 5 shows the calculated evolution of the magnetic field in time (and, equivalently, in space). The non-monotonic evolution of the
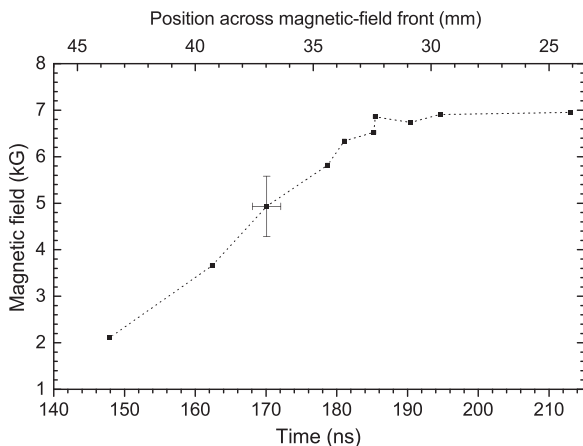

FIG. 5. The magnetic-field time evolution (and the deduced z dependence at $t = 160$ ns), at the dopant-plume center, determined using Eq. (5).

potential results in a spike ($t = 185$ ns) in the magnetic field profile. Even though this phenomenon is observed in the majority of the experiments, we cannot determine if it has implication on the nature of the magnetic-field penetration, since the jump is within the experimental uncertainty and it may also arise from a 2D or 3D effect. The measured magnetic field of $6.9 \pm 15\%$ kG at $t = 200$ ns, determined by the present method, is in agreement with the calculated field of $6.5 \pm 10\%$ kG, based on the measured current and geometry, as well as with the Zeeman splitting observation, reliably obtained at this time and z location.[15] At later times, the present diagnostic becomes impractical due to the low signal-to-noise ratio.

The width of the inferred magnetic-field front of $\sim$15 mm is nearly twice narrower than the previous lower-resolution estimates.[15] Yet, it is more than an order of magnitude wider than expected from the ideal models of specular reflection,[33] on the one hand, and the Hall-induced magnetic penetration,[16,17,19,20] on the other hand. The non-diffusive evolution of the magnetic field as a wave indicates a significant role for the Hall-induced mechanism in the penetration into the low charge-to-mass ratio plasma component. Assuming the presence of multi-species ions does not change the relation between the field-front width and the resistivity, the inferred width corresponds to a resistivity of $\eta = 4\pi v_b L_H/c^2 \sim 3 \times 10^{-13}$ s, where L_H is approximately half the front width.[34] The number of collisions during the passage time $\Delta t = L_H/v_b$ = 25 ns is $N = \nu\Delta t$, where $\nu = \eta n_e e^2/m_e$ is the collision frequency, so that $N = (L_H \omega_{pe}/c)^2$, ω_{pe} is the electron plasma frequency. For $n_e = 10^{14}$ cm^{-3} and $\nu = 8 \times 10^9$ s^{-1}, the large number of collisions, $N = 200$, allows the electrons to cross field lines in the current layer. It is emphasized that this resistivity estimate may not be valid, and a front-width prediction based on the observed complex physics requires a modified theory that will consider the role of the various ion species and their dynamics, as demonstrated for two ion-species in recent simulations[35,36] and in previous formulations.[37,38] In addition, energetic electrons emitted from the cathode may also affect the front width.[25,39,40]

The velocity of the propagating wave is comparable to both the hydrodynamic (Alfvén) velocity ($\sim$5 $\times 10^7$ cm/s) and the Hall-induced penetration velocity.[16] This is consistent with plasma pushing and field penetration, both observed simultaneously in our experiment. Whether the velocity is close to Alfvén velocity or governed by a Hall-induced penetration,[17] it is likely to be proportional to B_0, where B_0 is the magnetic field intensity at the generator side. When B_0 rises in time, as in our experiment, the velocity of propagation of the magnetic field is also expected to rise in time.[20] However, the magnetic field at the generator side only increases by $\sim$20% during the transit time of the current layer across the plume, and therefore, for this period of time the velocity should be constant to a good approximation, as was shown through the analysis of our measurements. In summary, a newly developed experimental spectroscopic approach enabled us to show that the magnetic field propagating through low-resistivity plasma penetrates the low charge-to-mass ratio component non-diffusively as a wave. The shape of the propagating field front is inferred with a

resolution comparable to the electron skin depth. The velocity of penetration is found to be much higher than expected from diffusion but not high enough to allow for field penetration into the entire multi-component plasma. This results in separation between penetrated low charge-to-mass ratio ion plasma and reflected high charge-to-mass ratio ion plasma. The resulting ion dynamics is shown to be consistent with the observed electron density. The inferred width of the narrow current layer (the magnetic-field front) can be useful for comparison with simulations that include the dynamics of multi-species plasma. Further research is also required to unfold the, likely present, small scale magnetic-field structures inside the current channel.

[1] J. Wesson and D. J. Campbell, *Tokamak* (Oxforde University Press, 1997).
[2] R. J. Commisso and H. R. Griem, Phys. Fluids **20**, 44 (1977).
[3] P. Bogen and E. Hint, in *Gaseous Electronics*, edited by M. N. Hirsh and H. J. Oskam (Academic Press, New York, 1978), Vol. 1.
[4] T. A. Mehlhorn, IEEE Trans. Plasma Sci. **25**, 1336 (1997).
[5] IEEE Trans. Plasma Sci. **PS-15** (1987), and references therein.
[6] W. Peter, A. Ron, and N. Rostoker, Phys. Fluids **26**, 2276 (1983).
[7] S. B. Mende, G. R. Swenson, S. P. Geller, J. H. Doolittle, G. Haerendel, A. Valenzuela, and O. H. Bauer, J. Geophys. Res.: Space Phys. **94**, 17063 (1989).
[8] M. J. Aschwanden, A. I. Poland, and D. M. Rabin, Annu. Rev. Astron. Astrophys. **39**, 175 (2001).
[9] K. J. H. Phillips, Plasma Phys. Controlled Fusion **42**, 113 (2000).
[10] C. Litwin, R. Rosner, and D. Q. Lamb, Mon. Not. R. Astron. Soc. **310**, 324 (1999).
[11] B. V. Weber, R. J. Commisso, R. A. Meger, J. M. Neri, W. F. Oliphant, and P. F. Ottinger, Appl. Phys. Lett. **45**, 1043 (1984).
[12] D. D. Hinshelwood, J. R. Boller, R. J. Commisso, G. Cooperstein, R. A. Meger, J. M. Neri, P. F. Ottinger, and B. V. Weber, Appl. Phys. Lett. **49**, 1635 (1986).
[13] M. Sarfaty, Y. Maron, Y. E. Krasik, A. Weingarten, R. Arad, R. Shpitalnik, A. Fruchtman, and S. Alexiou, Phys. Plasmas **2**, 2122 (1995).
[14] R. Shpitalnik, A. Weingarten, K. Gomberoff, Y. Krasik, and Y. Maron, Phys. Plasmas **5**, 792 (1998).
[15] R. Arad, K. Tsigutkin, Y. Maron, A. Fruchtman, and J. D. Huba, Phys. Plasmas **10**, 112 (2003).
[16] R. Doron, R. Arad, K. Tsigutkin, D. Osin, A. Weingarten, A. Starobinets, V. A. Bernshtam, E. Stambulchik, Y. V. Ralchenko, Y. Maron, A. Fruchtman, A. Fisher, J. D. Huba, and M. Roth, Phys. Plasmas **11**, 2411 (2004).
[17] A. S. Kingsep, Y. V. Mohkov, and K. V. Chukbar, Sov. J. Plasma Phys. **10**, 495 (1984).
[18] A. S. Kingsep, K. V. Chukbar, and V. V. Yankov, in *Reviews on Plasma Physics*, edited by B. Kadomtsev (Consultants Review, New York, 1990), Vol. 16, p. 243.
[19] A. Fruchtman, Phys. Fluids B **3**, 1908 (1991).
[20] K. Gomberoff and A. Fruchtman, Phys. Fluids B **5**, 2841 (1993).
[21] A. V. Gordeev, A. S. Kingsep, and L. I. Rudakov, Phys. Rep. **243**, 215 (1994).
[22] A. Chuvatin and B. Etlicher, Phys. Rev. Lett. **74**, 2965 (1995).
[23] D. Hinshelwood, B. Weber, J. M. Grossmann, and R. J. Commisso, Phys. Rev. Lett. **68**, 3567 (1992).
[24] E. M. Waisman, P. G. Steen, D. E. Parks, and A. Wilson, Appl. Phys. Lett. **46**, 1045 (1985).
[25] J. M. Grossmann, P. F. Ottinger, J. M. Neri, and A. T. Drobot, Phys. Fluids **29**, 2724 (1986).
[26] J. M. Grossmann, P. F. Ottinger, and R. J. Mason, J. Appl. Phys. **66**, 2307 (1989).
[27] A. Fruchtman, J. Grossmann, S. Swanekamp, and P. Ottinger, IEEE Trans. Plasma Sci. **27**, 1464 (1999).
[28] A. Weingarten, R. Arad, Y. Maron, and A. Fruchtman, Phys. Rev. Lett. **87**, 115004 (2001).
[29] R. Arad, K. Tsigutkin, Y. Maron, and A. Fruchtman, Phys. Plasmas **11**, 4515 (2004).
[30] R. Arad, K. Tsigutkin, Y. V. Ralchenko, and Y. Maron, Phys. Plasmas **7**, 3797 (2000).
[31] J. F. Friichtenicht, Rev. Sci. Instrum. **45**, 51 (1974).
[32] B. Rubinstein, R. Doron, J. Citrin, R. Arad, Y. Maron, A. Fruchtman, H. R. Strauss, and T. A. Mehlhorn, "Electron density evolution during a fast, non-diffusive propagation of a magnetic field in a multi-ion-species plasma," Phys. Plasmas (unpublished).
[33] M. Rosenbluth, in *Progress in Nuclear Energy, Series XI*, edited by J. T. C. L. Longmire and W. B. Thompson (Pergamon, London, 1963), Vol. 2.
[34] A. Fruchtman and L. I. Rudakov, Phys. Rev. Lett. **69**, 2070 (1992).
[35] H. R. Strauss, R. Doron, R. Arad, B. Rubinstein, Y. Maron, and A. Fruchtman, Phys. Plasmas **14**, 053504 (2007).
[36] A. Richardson, J. Angus, S. Swanekamp, P. Ottinger, and J. Schumer, IEEE Trans. Plasma Sci. **42**, 2552 (2014).
[37] G. Barak and N. Rostoker, Appl. Phys. Lett. **41**, 918 (1982).
[38] A. V. Gordeev, Plasma Phys. Rep. **27**, 659 (2001).
[39] P. F. Ottinger, S. A. Goldstein, and R. A. Meger, J. Appl. Phys. **56**, 774 (1984).
[40] R. J. Mason, M. E. Jones, J. M. Grossmann, and P. F. Ottinger, Phys. Rev. Lett. **61**, 1835 (1988).